PCCP

Accepted Manuscript

ROYAL SOCIETY OF CHEMISTRY

www.rsc.org/pccp

Journal Name Physical Chemistry Chemical Physics Dynamic Article Links ►

Cite this: DOI: 10.1039/c0xx00000x

www.rsc.org/xxxxxx

ARTICLE TYPE

Magnetic Edge-state in Nanographene, HNO_3-Doped Nanographene and Its Residue Compounds of Nanographene-based Nanoporous Carbon

Si-Jia Hao,[a] V. L. Joseph Joly,[a] Satoshi Kaneko,[a] Jun-ichi Takashiro,[a] Kazuyuki Takai,[a†] Hitoshi Hayashi,[b] Toshiaki Enoki,[a*] Manabu Kiguchi[a*]

Received (in XXX, XXX) Xth XXXXXXXXX 20XX, Accepted Xth XXXXXXXXX 20XX
DOI: 10.1039/b000000x

We investigated the magnetic and electronic properties of nanographene and its charge transfer effect, using near edge X-ray absorption fine structure (NEXAFS), magnetic susceptibility, ESR, and elemental analysis, with the employment of nanoporous carbon, which consist of a three dimensional disordered network of loosely stacked nangraphene sheets, in relation to the host-guest interaction with HNO_3 as electron-accepting guest. The adsorption of electron acceptor HNO_3 decreases the intensity of the edge state peak in NEXAFS as a result of the charge-transfer-induced Fermi energy downshift, in agreement with the decrease in the edge-state spin concentration, and it also induces the structural expansion, which makes the inter-nanographene sheet distance elongated, resulting in weakening the inter-nanographene-sheet antiferromagnetic interaction as evidenced by the decrease in the Weiss temperature. In addition, the decomposition of HNO_3, which takes place with the electron-rich edge state as oxidation catalyst, results in the creation of oxygen/nitrogen-containing functional groups bonded to the periphery of the nanographene sheets. Heat-treatment of the HNO_3-ACFs under evacuation desorbs the HNO_3 molecules completely, though a part of the oxygen/nitrogen-containing species remains strongly bonded to the edge even at high temperature of ~800 ˚C, according to NEXAFS and elemental analysis results. These remaining species participate in the charge transfer, modifying the electronic structure as observed with the decrease in the orbital susceptibility and the strengthening of the inter-nanographene-sheet antiferromagnetic interaction.

1. Introduction

Graphene, 2D one-atom-thick monolayer of carbon atoms arranged in a honeycomb lattice, has recently attracted tremendous interests from the scientific community for both fundamental and applied researches owing to its unconventional electronic structure of massless Dirac fermions[1,2] which gives rise to unprecedented physical properties such as the room-temperature half-integer quantum Hall effect, the extremely high mobility of its charge carriers, the tunable band gap of graphene nanoribbons, and the potential for realizing ballistic conduction.[3,4] These unique physical properties lead graphene as a challenging basis for applications in electronic devices[5], biosensors[6], field effect transistors[7] and fuel cells[8].

When an infinite graphene sheet is cut into nanoscale size fragments, nanographene such as graphene nanoisland or graphene nanoribbon is created.[9-12] Here, the periphery of nanographene is described in terms of a combination of zigzag and armchair edges. According to theoretical predictions[13-18], the electronic structure of nanographene is strongly modified from infinite graphene depending on the edge geometry, and importantly, an edge-state that is localized on the zigzag-shaped edge is created, in spite of the absence of such state on the armchair edge. The edge state, which is nonbonding π-orbital at the Fermi level and has a large local density of states in the zigzag edge region, is electronically and chemically active. In addition, the localized spin inherent of edge state is responsible for the magnetic activity of nanographene, and it is quite sensitive to charge transfer interaction of nanographene with guest molecules because it is positioned at the Dirac point, at which the conduction π*-bands and valence π-bands touch each other.[19] Therefore in addition to the bidirectional nature of charge transfer between donor and acceptor, which is similar to the infinite graphene and bulk graphite[19], the active edge-state plays an important role in the electronic, chemical and magnetic processes in nanographene.

Under the direction of these theoretical predictions, the presence of edge state on the edges of finite size graphene has been evidenced experimentally by using various kinds of techniques, such as scanning

tunneling microscopy/spectroscopy (STM/STS)[20-22], energy loss near edge fine structure (ELNES) spectra[23] and magnetic force microscopy[24,25]. Recently near edge X-ray absorption fine structure (NEXAFS) studies reported the observation of the edge-state on the nanographene[26,27], and our group confirmed the magnetic feature of the edge state on the basis of a combination of NEXAFS and magnetic techniques (ESR and magnetic susceptibility) with graphene nanoribbons[28] and fluorinated nanographites[29].

Among recent researches on the detailed electronic and magnetic properties of edge state contributing to the magnetism of nanographene, a focus has been placed on the role of edge state in interaction between nanographene and guest molecules, and interesting magnetic features have been found in the nanographene-based host guest systems with an employment of activated carbon fibers (ACFs) that is nanographene-based nanoporous carbon.[30-32] The structure of ACFs features a disordered flexible 3D network of nanographite domains, each of which consists of a loose stacking of 3 to 4 nanographene sheets with a mean in-plane size of 2 to 3 nm. This unique hierarchical structure consisting of nanographene sheets is reflected on the magnetic structure of ACFs. Indeed, previous studies[33,34] allow us to understand the detailed magnetic structure as follows.

The constituent nanographene sheet with its periphery being a combination of zigzag and armchair edges has edge-state spins ferromagnetically coupled with each other in a single zigzag edge through strong ferromagnetic intra-zigzag-edge interaction having a strength of several 10^3 K. The edge-state spins in one zigzag edge are interacting with the edge-state spins in the neighboring zigzag edges through intermediate strength antiferromagnetic/ferromagnetic inter-zigzag-edge interaction (several 10-10^2 K). As a result of the compensation between the ferromagnetic spin clusters in neighboring zigzag edges, between which non-magnetic armchair edges are embedded, the individual nanographene sheet has ferrimagnetic structure with a non-zero net magnetic moment. The network structure of nanographene sheets gives another detail in the magnetic structure of ACFs in relation to the inter-nanographene interaction and inter-nanographite-domain interaction.[32,33] In individual nanographite domains of the ACF network structure, between which nanopores are formed, weak antiferromagnetic inter-nanographite-domain interaction of several K couples edge-state spins between nanographite domains. The edge-state spins of adjacent nanographene sheets loosely stacked in an individual nanographite domain, where the gallery between constituent nanographene sheets is too narrow to accommodate physisorptive guest molecules, are coupled with each other through weak antiferromagnetic inter-nanographene interaction, whose strength is stronger than that of inter-nanographite-domain interaction.

The interstitial nanopores in ACFs can accommodate various kinds of guest molecules with the aid of van der Waals interaction and charge transfer interaction.[32-37] Among the guest molecules investigated so far, HNO_3 is particularly interesting from the following reasons.[38,39] The adsorption of HNO_3 shows a stepwise charge transfer from nanographene to acceptor HNO_3, which can be tracked by the decrease in the edge-state spin concentration, due to the aforementioned structural hierarchy in ACFs.[33] Here the interplay between the charge transfer and adsorption-induced mechanical expansion of the nanopores is responsible for this stepwise behavior. Meanwhile the decomposition of HNO_3 molecules takes place upon the interaction with nanographene sheet, in which the active edge-state electrons play a catalytic role, giving magnetic NO molecules, which are strongly confined into the nanopores and dimerized at low temperature.[34] What is important here in the interaction with HNO_3 is that the desorption behavior of HNO_3 molecules is different from that of other guest molecule cases. Even intensive heat treatment at 200 ^{o}C cannot completely remove the guest species, resulting in remaining oxygen/nitrogen-containing species such as nitro groups strongly bonded to nanographene sheet. Due to this feature specific to HNO_3, the understanding of the electronic structure of the edge state in the HNO_3 doped ACFs remains a problem at this moment and its behavior under heat-treatment is not clearly understood.

To understand more comprehensively the behavior of edge-state electrons in the nanographite system, in the present research we investigated the electronic structure and magnetic properties of the edge-state in relation to the host-guest interaction with HNO_3 as acceptor and heat-induced decomposition of the host-guest system using the nanographite system (ACFs), HNO_3 doped nanographite (HNO_3 adsorbed ACFs) and its residue compounds through element analysis, NEXAFS, static magnetic susceptibility and ESR measurements.

2. Experimental

Phenol-based ACFs (Kuractive FR-20, Kuraray Chemical Co., Ltd.) with specific surface areas of about 2000 m^2/g were heat-treated at 200 ^{o}C for 72 h, in the vacuum of at least 10^{-6} Torr to remove as-adsorbed foreign gaseous species, mainly to avoid the magnetic oxygen which could affect the magnetic measurements. Fuming nitric acid solution (Wako Pure Chemical Industries, Ltd.) with a volume fraction higher than 97% was purified by the freeze-pump-thaw method prior to the adsorption process.

Only HNO_3 was considered to be adsorbed into the ACFs, as the water content was negligible in the vaporized gas from such fuming nitric acid solution.[40] The nitric acid adsorbed samples (HNO_3-ACFs) were prepared by placing the ACFs in the HNO_3 gas shower at room temperature and the duration of the adsorption was at least 2 h which was enough to reach the equilibrium. In addition, the residue compounds (RC) were made by evacuating these as-prepared HNO_3-ACFs samples to ~ 10^{-6} Torr again at room temperature (RC-RT), 100 °C (RC-100), 200 °C (RC-200), 300 °C (RC-300), 400 °C (RC-400), 500 °C (RC-500), 600 °C (RC-600) and 800 °C (RC-800) for 12 hours. Meanwhile by contrast, the non-adsorbed ACFs (ACFs-200) also went through a heat treatment at 300 °C (ACFs-300), 400 °C (ACFs-400), 500 °C (ACFs-500), 600 °C (ACFs-600) and 800 °C (ACFs-800) for 12 hours under ~ 10^{-6} Torr. Then the element analysis (combustion method) on carbon, nitrogen and hydrogen was carried out for the ACFs and RC samples, where the residual content is considered to be oxygen since the samples are simply composited by CHNO.

After typically 20 mg sample was vacuum sealed, its magnetic susceptibility was measured by SQUID magnetometer (MPMS5, Quantum Design) at 2 T between 2 and 300 K. The sample weight could be estimated from the weight difference between the glass tube with the sample sealed inside and the empty glass tube, for the latter of which the weight was measured after the sample was taken out. ESR spectra were investigated at room temperature with a microwave power of 1 mW for the ACFs and RC samples (about 2 mg) vacuum-sealed in a quartz tube by using JEOL JES-TE200 X-band spectrometer. The fabric axes of bundled fibers were oriented perpendicular to the electric field direction of the microwave in the ESR cavity (TE_{001} cylindrical) for avoiding the skin depth effect of the measurements. The accuracy of magnetic field in the ESR measurements was calibrated by using DPPH as a reference.

The NEXAFS spectra of carbon, nitrogen and oxygen K-edge were measured at the soft x-ray beam line BL-7A in the Photon Factory in the Institute of Materials Structure Science (Tsukuba, Japan). The as-prepared samples (non-adsorbed ACFs and HNO_3-ACFs) were taken out from the glass tube and mounted on a Ta plate and loaded onto the sample holder, then this sample holder was introduced into the chamber maintained in ultrahigh-vacuum (10^{-9} Torr) as soon as possible, and the samples are labeled as ACFs-RT and RC-RT. NEXAFS spectra around the carbon, nitrogen and oxygen K-edge were obtained in total electron yield mode, and the photon energy was calibrated with respect to the C1*s*-π^* peak position of highly oriented pyrolytic graphite (HOPG) at 285.5 eV. Then in the chamber the samples underwent heat treatments at 100 °C (ACFs-100 and RC-100), 200 °C (ACFs-200 and RC-200), 300 °C (ACFs-300 and RC-300), 400 °C (ACFs-400 and RC-400), 500 °C (ACFs-500 and RC-500), 600 °C (ACFs-600 and RC-600) and 800 °C (ACFs-800 and RC-800) in the vacuum of 10^{-9} Torr for 30 minutes, and the spectra of carbon, nitrogen and oxygen K-edge were recorded respectively.

3. Results and Discussion

Figure 1(a) gives the carbon K-edge NEXAFS spectra of the RC samples which are made at different temperatures under evacuation, and all these spectra are normalized by the carbon edge jump around 350 eV for comparison, with the calibration to the π^* peak position of HOPG. Three main features are observed in the series of carbon spectra. Firstly all the samples show a dominant peak at ~285.5 eV, which agrees with the C1*s*-to-π^* (C=C) transition of HOPG, suggesting the underlying graphitic structure in the samples. Secondly the peak located around 292.5 eV can be attributed to the energy of C1*s*-to-σ^* (C–C) transition (HOPG 291.85 eV). In addition one more peak (~289.0 eV) is present between the π^* and σ^* peak, which is usually assigned to the sp^2 carbon connected to the carbon bonded to hetero-atoms (X=N, O, H) in the –C=C–X configuration.[41] Such feature is enhanced as the heating temperature increases to over 400 °C however it is much depressed while heated to 800 °C, indicating the formation and removal of the aforementioned carbon bonding configuration.

The close-up view of the C1s π^* region is given in Figure 2 for the ACFs-RT, RC-RT and HOPG, with the photon energy between 282 eV and 287 eV. In addition to that a slight upshift of the π^*-state peak (~ 0.15 eV) is observed in the ACF-RT and RC-RT from that of HOPG, it is clear to see that, compared to the HOPG, a shoulder located on the low-energy side of the π^*-state peak of the ACF-RT and RC-RT is present, demonstrating one additional unoccupied state in the vicinity of the Fermi level in the ACFs and its residue compounds.[28,29] Moreover as shown in Figure 2, the feature of such unoccupied state is enhanced for the evacuated HNO_3-ACFs sample at room temperature (RC-RT).

As discussed in references 28 and 29, two potential origins could result in this additional unoccupied state; dangling bonds of σ-electron and/or edge-state of π-electron. Since the samples were placed in the vapor of nitric acid which behaves as a strong oxidizer, the dangling bonds, if they existed, must have been consumed to form oxygen-/nitrogen-containing functional groups. Besides the extra peak in between π^* and σ^* in Figure 1(a), indicating carbon bonding with hetero-atoms, suggests the absence of dangling bonds. Therefore, this additional unoccupied state could be assigned to the edge-state.

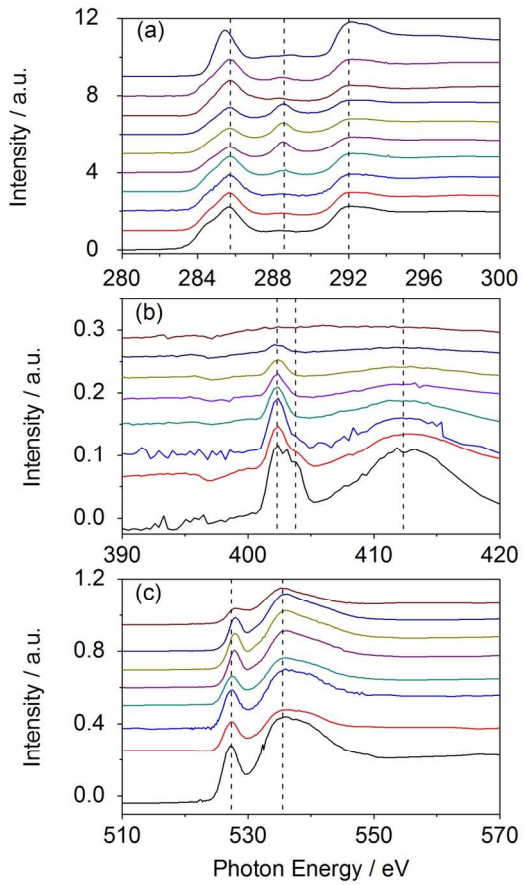

Figure 1 The carbon (a), nitrogen (b) and oxygen (c) K-edge NEXAFS spectra of residue compounds vacuum-heated at different temperatures. In each figure from the bottom to the top, the samples are labeled as RC-RT, RC-100, RC-200, RC-300, RC-400, RC-500, RC-600 and RC-800, respectively. The carbon K-edge spectra of HOPG and ACFs-RT are shown, respectively, at the top and the second from the top in (a).

In order to understand the detailed behavior of the edge-state, the pre-edge region in the carbon K-edge spectrum (282–287 eV) is deconvoluted into a combination of two Gaussian peaks corresponding to the edge-state (284.34 eV, Γ=1.05 eV) and the π* state (285.47 eV, Γ=1.58 eV) and a step function (285.48 eV, Γ=0.54 eV) for the RC and ACFs samples. Here the fixed energy for each function is adopted, because the heat treatment does not change significantly the carbon π electron configuration in the nanographite system. Figure 3 gives these deconvolution results of non-adsorbed ACFs (ACFs-200) and the residue compounds (RC-RT and RC-800), which clearly show that the contribution of edge-state is much depressed due to the heating under vacuum for the RC samples. Such suppressive effect becomes more visible in the Figure 4(a), where the edge-state intensity is shown. Here, the edge-state intensity is defined as the area of peak corresponding to the edge state in NEXAFS spectra. When the ACFs samples are heated up to 800 °C, the strength of the edge-state with respect to that of the π* state fluctuates around the average value ~0.12, which again confirms the thermal stability of nanographite against heating, mainly because it has already experienced high temperature activation at 800 °C.[42] The RC-RT sample gives the largest value of edge-state strength (~0.31±0.06). Taking into account that the strength of the peak represents the ratio of states, which are not occupied, the largest value demonstrates that the edge state is most vacant in the RC-RT sample. The introduction of HNO_3 into ACFs leads to the downshifted Fermi energy through the charge transfer from nanographene to HNO_3, resulting in the increase of the unoccupied state in the edge-state due to the creation of vacancies. This experimental finding suggests that, even after evacuation at room temperature, the remaining HNO_3 acceptor molecules grab electrons from the edge states, giving the largest contribution of the edge state in the NEXAFS spectrum of the RC-RT sample. Interestingly, when the heating temperature to the RC samples increases, the relative edge-state intensity is weakened from ~0.31 (room temperature) to ~0.07 (800 °C), and the latter one is close to the average value of the non-adsorbed ACFs samples. This behavior indicates that the vacuum heating could remove the charge-transfer species, namely the Fermi energy of nanographene shifts back to the Dirac point, and then the electronic structure is recovered to be the same as the non-adsorbed ACFs.

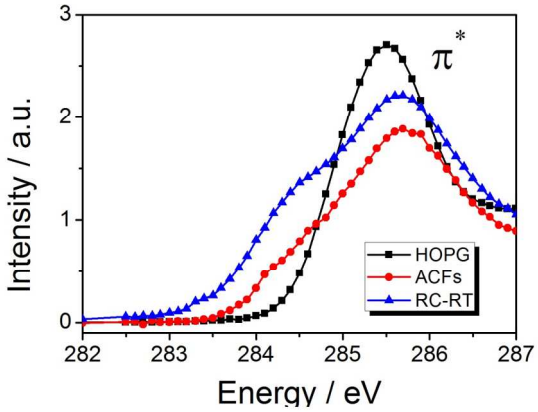

Figure 2 The close-up of the carbon K-edge NEXAFS in the π* region of the carbon 1s edge between 282 eV and 287 eV for the ACFs (ACFs-RT), the residue compound treated at room temperature (RC-RT) and HOPG.

The nitrogen and oxygen K-edge NEAXFS spectra (Figures 1(b) and (c), respectively) could be easily understood with the help of the element analysis

results for the ACFs, HNO_3-ACFs and RC samples, which are converted to the atom number of hydrogen, nitrogen and oxygen on a piece of nanographene sheet constituted by around 350 carbon atoms (in-plane size of ~3 nm) in Figure 5. As shown in Fig.5, the saturation of HNO_3 into the ACFs (HNO_3-ACFs) gives around 22 nitrogen atoms due to the adsorption and intercalation of HNO_3 molecules[39], in contrast to the absence of nitrogen in the non-adsorbed ACFs since the nitrogen-free phenol based precursor[42]. Here the estimated atom ratio between nitrogen and carbon is about 0.06, which is much lower than the maximum HNO_3 concentration $HNO_3/C \sim 0.204$ in the previous report.[39] This may be because either such high HNO_3 concentration in the latter sample is achieved through absorption at the boiling point of HNO_3 or desorption takes place in the former one while the sample exposed to the air in a short time. In the nitrogen K-edge NEXAFS spectra (Fig. 1(b)), in addition to the N1s-to-σ* transition peak at 412 eV, the N1s-to-π* transition gives two peaks at 402.4 and 403.8 eV, which become silenced above the RC-800 and RC-300 sample, respectively. The feature of sharp π* peak and large gap between π* and σ* resonances are reported for cases of nitrate ($-NO_3^{-1}$) and nitro group ($-NO_2$), the latter of which is more strongly bonded than the former.[43] In connection with the fact (given in reference 39 and evidenced in Fig.5(b)) that in the RC-RT/RC-200, a part/almost all of NO and HNO_3 molecules are removed, the peak at 403.8 eV which disappeared in the RC-300 could be assigned to be the nitrate groups. Then another peak at 402.4 eV is attributed to be the nitro groups[34], which could be removed after 800 °C heating as shown in Fig.1(b). Due to the low intensity of the measured spectra, up to now the quantitative analysis is too difficult to perform, however it is obvious that as the heating temperature elevates to 800 °C, the intensity of all these peaks is depressed and vanished, demonstrating almost all of the nitrogen is removed from the RC samples. It should be noted that this is somehow a contradiction with the element analysis results that a very few amount of nitrogen survived in the RC-800 sample. A trace of nitrogen present as evidenced here plays a role in the modification of magnetic behavior of edge-state spins, as we will discuss later.

In the non-adsorbed ACFs, the presence of hydrogen and oxygen atoms (Figs. 5(a) and 5(c)) suggests that the peripheries of the constituent nanographene sheet are decorated with oxygen/hydrogen-containing functional groups. This is consistent with the mass spectra in the decomposition process of the non-adsorbed ACFs at 200 °C, as it indicates that strongly bonded functional groups such as phenol (–OH) and carbonyl (>C=O) groups remain bonded after heat-treatment though most carboxyl (–COOH) groups are removed.[44] In addition, the slightly shifted contents of the hydrogen and oxygen in the ACFs series samples due to the heating up to 800 °C are consistent with the fact that the samples have already experienced thermal annealing at 800 °C.[42]

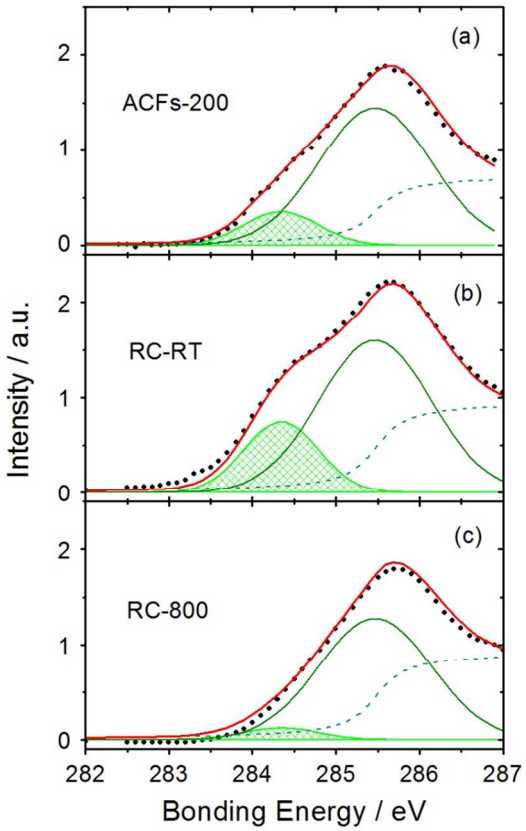

Figure 3 The close-up view of the π* region of the carbon 1s edge between 282 eV and 287 eV for the (a) non-adsorbed ACFs (ACFs-200), and residue compounds (b) RC-RT and (c) RC-800. The data points are indicated in solid circles and the convoluted curve fit is presented by the thick red line. The deconvolution of the spectra comprises two Gaussian peaks corresponding to the edge-state (shadowed, 284.34 eV) and the π* state (unshaded, 285.47 eV), and a step-function (dash curve, 285.48 eV).

For the HNO_3-ACFs, largely elevated contents of hydrogen and oxygen, which are much more than the increment of nitrogen, are observed and they can be understood on the basis of the oxidation of the edge carbon atoms due to the strong oxidizability of HNO_3. Typically one round piece of ~3 nm nanographene sheet is constituted by ~ 350 carbon atoms, in which about 1/4 namely ~ 90 atoms are distributed on the periphery. Therefore such high H and O contents for the HNO_3-ACFs suggest that the nanographene edges at which carbon atoms are decorated with oxygen-containing functional groups having affinity to water are subjected to the adsorption of a large amount of water. This conjecture is verified by the fact that the heat treatment of the HNO_3-ACFs up to 300 °C under vacuum results in rapid reduction in large amounts of

hydrogen and oxygen contents, in which the atom number ratio between them at RT - ~200 ˚C is 1.5-1.8 close to 2, as shown in Fig.5. The deviation from 2 might indicate the removal of some other functional groups such as carboxyl (–COOH), accompanied with the nitrogen-containing guest molecules or groups. Then such reduction becomes moderate and the contents of hydrogen and oxygen are recovered to those of the non-adsorbed ACFs when the heating temperature is above 300 °C for the residue compounds.

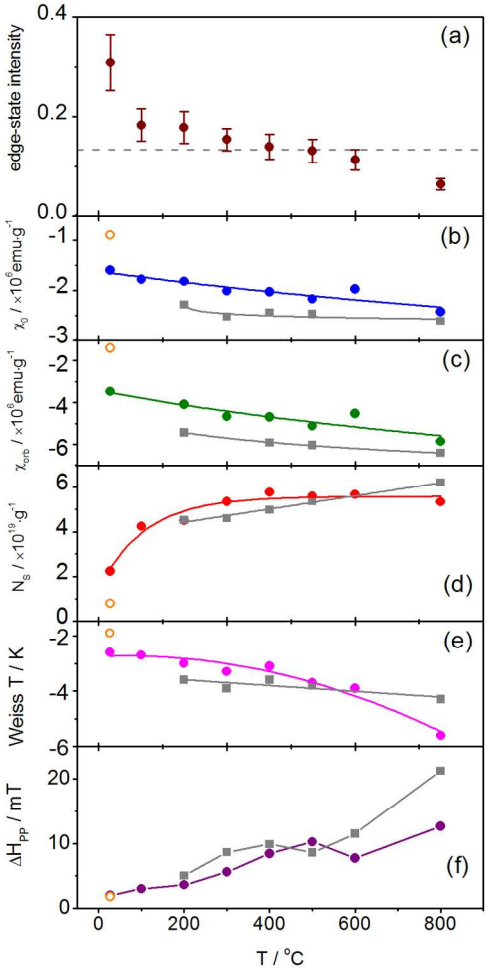

Figure 4 The derived intensity ratio of edge-state to π* state (a), temperature-independent magnetic susceptibility term χ_0 (b), orbital magnetic susceptibility (c), the concentrations of edge-state spins (N_S) (d), Weiss temperature (e), and ESR linewidth (ΔH_{pp}) (f) as a function of heating temperature for the non-adsorbed ACFs (grey solid squares) and the residue compounds (colored solid circles). The corresponding value of the HNO_3 saturated ACFs is also shown in the figure as the orange ring. The solid lines are guides for the eyes. The dashed line in (a) denotes the average value of ACFs samples heat-treated at temperatures of 400-800 ˚C.

The oxygen K-edge spectra for the RC samples shown in Fig.1(c) display two peaks, 527.2 eV and 536.5 eV, which are assigned to the O1*s*-to-π* transition and O1*s*-to-σ* transition, respectively. The intensities of both peaks are reduced due to the heating, suggesting the removal of oxygen from the system, which is consistent with the element analysis results in Fig. 5(c). Meanwhile upon the heating, the spectra give two features; small upshift of the π* peak and the sharpening of the σ* peak especially above 300 °C. In the case of graphene oxide membranes, it is reported that the π* excitation energy of C–O (534 eV) is higher than that of C=O (531.5 eV), in spite of the opposite trend for the σ* excitation energy (540 and 542 eV).[45] In addition the enhanced middle peak (~289.0 eV) in the C K-edge spectra (Fig. 1(a)) upon the rising temperature up to 600 °C suggests the increment of carbon which is single bonded. Therefore the behavior of O K-edge for the RC samples indicates that the heating in this temperature range works to create C–O at the expense of C=O. In other words, the majority of oxygen-containing functional groups bonded to edge carbon atoms becomes evolved from carbonyl-type to phenol-type in the heat-treatment temperature range up to 600 °C. Moreover, the decrease in the middle peak in the C K-edge spectra above 600 °C is understood as the change in the edge decoration from phenol-bonded edge to hydrogen-terminated edge.

Let us discuss the magnetic properties which vary upon interplay between the reaction with HNO_3 and the subsequent heat treatment. Figure 6 shows the temperature dependence of the static magnetic susceptibility of the non-adsorbed ACFs and the residue compounds, both of which are heat-treated up to 800 °C, together with that of the HNO_3-ACFs. As discussed comprehensively in the previous reports[33,34], the observed static magnetic susceptibility (χ_{obs}) of the heat-vacuumed non-adsorbed ACFs is represented as a combination of temperature-dependent spin term $\chi_S(T)$ and temperature-independent term χ_0. Here the edge-state spin governs the spin susceptibility, which follows the Curie-Weiss law $\chi_S(T) = C/(T-\Theta)$ (C; the Curie constant, Θ; the Weiss temperature), and the term χ_0 consists of orbital magnetism χ_{orb} and core diamagnetism. Figure 4 summarizes the heat-treatment temperature dependence of the magnetic data for the ACFs and the residue compounds. Here we focus first on the orbital susceptibility χ_{orb} for investigating the variation of the electronic properties upon the sample treatments. The orbital susceptibility χ_{orb}, which is obtained by subtracting the core diamagnetism from the observed χ_0 on the basis of the Pascal rule and the elemental analysis (Fig.5), is given in Fig.4(c) as a function of heat treatment temperature together with χ_0 (Fig.4(b)). χ_{orb} is negative, and its absolute value is independent of the heat treatment temperature above 300 °C for the non-adsorbed ACFs and is always larger than that of the residue compounds and HNO_3-ACFs. The large negative value indicates that extended π-conjugated system features the electronic structure of the constituent nanographene sheets in the non-adsorbed

ACFs independent of the heat treatment temperature. In the heat treatment temperature range above 300 °C, most of the oxygen-containing functional groups are removed as evidenced in the elemental analysis in Fig.5. Accordingly the Fermi level can be located in the vicinity of the Dirac point due to the weakened charge transfer from the nanographene sheets to these functional groups bonded to the edge carbon atoms. Theoretical works[46] on the orbital susceptibility of graphene proves that the absolute value of χ_{orb} is maximum when the Fermi level is placed at the Dirac point and it sharply decreases as it goes far from the Dirac point. The trend in χ_{orb} with the comparison between the non-adsorbed ACFs, and the residue compounds and HNO_3-ACFs, where the latter two are subjected to the charge transfer to the oxygen/nitrogen-containing functional groups and HNO_3 guest molecules, confirms the behavior predicted by the theory. Here, let us see the detailed behavior of the orbital susceptibility of the residue compounds and HNO_3-ACFs. The smallest absolute value in the HNO_3-ACFs indicates the presence of strong charge transfer effect with strong acceptor HNO_3 molecules intercalated into the galleries of nanographene sheets and accommodated into the nanopores. The vacuum heat treatment, which works to remove the HNO_3 molecules, increases the absolute value of χ_{orb}. The absolute value is increasing monotonically as the heat treatment temperature is elevated. This proves that oxygen/nitrogen-containing functional groups, which act as electron accepting species, are removed successively. However, the value is still smaller than that of the non-adsorbed ACFs even at 800 °C. Taking into account the elemental analysis result shown in Fig.5, this importantly suggests the presence of a trace of oxygen/nitrogen-containing functional groups, which operates in the charge transfer from the constituent nanographene sheets.

The charge transfer effect with HNO_3 and oxygen/nitrogen-containing functional groups, which we observed in the orbital susceptibility, is confirmed by the result of the edge-state intensity in the NEXAFS spectra as already discussed with Fig.4(a). Indeed, the NEXAFS spectra together with the elemental analysis indicate the following scenario on the charge transfer and the modification of the electronic structure. In the low temperature range below 200-300 °C, strong acceptor species of NO_3^- ions accommodated in the galleries of nanographene sheets and nanopores participate in the charge transfer in addition to the contribution of oxygen-containing functional groups such as –COOH and >C=O bonded to edge carbon atoms, while, above that temperature range, functional groups such as –OH and $–NO_2$ participate in the charge transfer process. However, in the higher temperature range around 800 °C, the contribution of these groups becomes small, and only nitrogen atoms strongly bonded to the edge carbon atoms and incorporated into the graphene sheet modify the electronic structure, resulting in the less conjugated π-electronic state.[42]

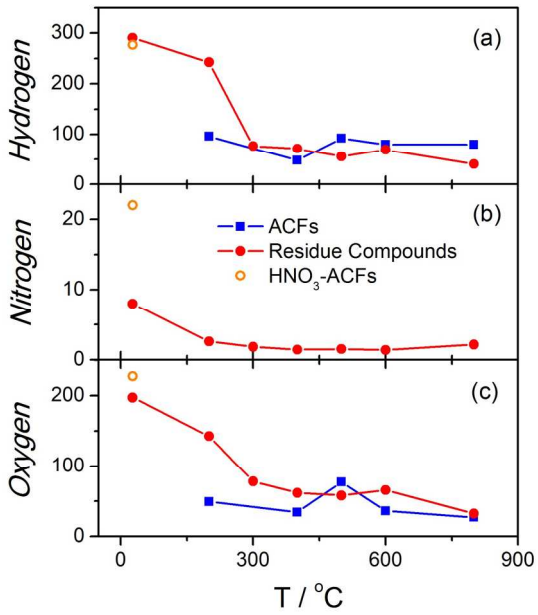

Figure 5 The elementary analysis results of the ACFs and residue compounds samples, it is conversed to the atom number of hydrogen (a), nitrogen (b) and oxygen (c) on a nanographene sheet whose in-plane size is 3 nm (about 350 carbon atoms). The data of HNO_3 saturated ACFs is plotted here for comparison.

Now our task on the magnetism is the role of edge-state spins. Figures 4(d) and (e) show the heat-treatment temperature dependence of the spin concentration χ_S and the Weiss temperature Θ, respectively for the non-adsorbed ACFs, HNO_3-ACFs and the residue compounds. In the non-adsorbed ACFs, the spin concentration increases monotonically from 4.5 to 6.2×10^{19} g^{-1} when heat treated from 300 to 800 °C. This indicates that a trace of oxygen-containing functional groups, which are still bonded to the edge carbon atoms and consequently work to take electrons from the interior of nanographene sheets, are removed in the heat-treatment above 300 °C. The edge-state spin concentration accordingly becomes increased as the Fermi level approaches the Dirac point. The weakly antiferromagnetic Weiss temperature Θ ~ −4 K, for which the inter-nanographite-domain interaction is responsible, is independent of the heat treatment temperature in the entire temperature range.[33] The inter-nanographite-domain antiferromagnetic interaction is not seriously affected by the heat treatment in this temperature range because the environment surrounding the nanographite-domains does not change so seriously as evidenced by the fact that the amount of oxygen-containing functional groups bonded to the edge carbon atoms does not vary so much (Fig.5).

Similar to the ACFs samples, the HNO_3-ACFs and RC samples exhibit the Curie-Weiss behavior of their magnetic susceptibility except the presence of an additional contribution which increases above 200 K for HNO_3-ACFs and RC-RT as shown in Fig.6(d). The additional contribution is assigned to magnetic NO molecules (S=1/2) created in the decomposition of HNO_3 molecules, in which the electron-rich edge state plays an important catalytic role, as discussed in the previous report.[39] The behavior exhibited in Fig. 6(d) proves that the NO molecules are completely removed when the sample is heat treated above 200 °C.

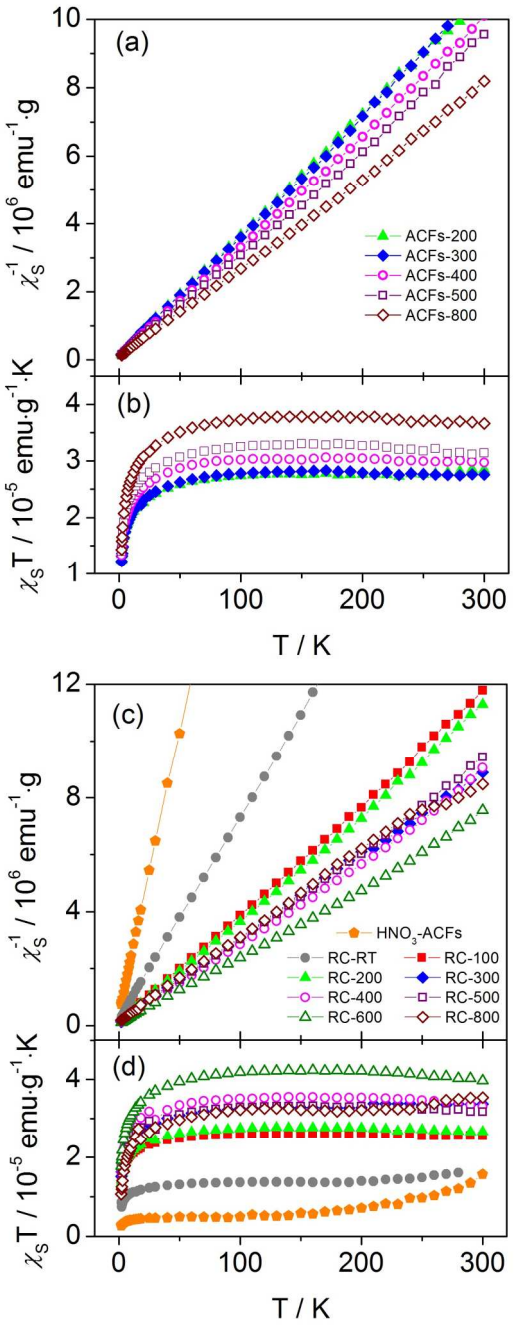

Figure 6 The temperature dependence of the reciprocal spin susceptibility χ_S^{-1} and the product of χ_ST for the ACFs (a, b) and residue compounds samples (c, d) which are vacuumed and heated at different temperatures. The spin susceptibility χ_S is obtained after subtracting the temperature-independent term χ_0 from the observed susceptibility.

Figures 4(d) and (e) summarize the spin concentration and the Weiss temperature of the residue compounds and HNO_3-ACFs. The edge-state spin concentration N_S is sharply depressed from ~4.5×10^{19} to ~ 0.8×10^{19} g^{-1}, after the introduction of HNO_3 into ACFs (Fig. 4(d)) as a result of charge transfer interaction from nanographene to strong electron acceptor HNO_3. Evacuation at room temperature and 100 °C works to bring HNO_3-ACFs back to the non-adsorbed state in spite that a small amount of NO_3^- species having acceptor nature remain participating in the charge transfer, as we observe that the spin concentration increases toward that of the non-adsorbed ACFs. Above 300 °C, the spin concentration goes back to that of the non-adsorbed ACFs. This is consistent with the finding that most of oxygen, hydrogen and nitrogen contents which are associated with the functional groups of the HNO_3 guest origin, are removed in this low temperature range. The spin concentration (5.5×10^{19} g^{-1}) is almost independent of the heat treatment temperature in the higher temperature range above 300 °C, where the chemical environment becomes stabilized with less functional groups bonded to the edge carbon atoms. What is interesting here is the heat-treatment-induced change in the Weiss temperature and the decrease of the Weiss temperature in the residue compounds and the HNO_3-ACFs, respectively. The HNO_3-ACFs have a Weiss temperature of □2 K, whose absolute value is smaller than that of the non-adsorbed ACFs. The HNO_3 molecules accommodated in the nanopores between nanographite domains and the galleries between nanographene sheets act to make nanographene sheets apart from each other. Accordingly, the decrease in the absolute value of the Weiss temperature, which represents the strength of inter-nanographite-domain antiferromagnetic interaction, can be explained in terms of this structural expansion induced by the adsorption of HNO_3 guest molecules.[34,35,38] The absolute value of the Weiss temperature in the residue compound obtained at room temperature evacuation is larger than that of HNO_3-ACFs. This is in good agreement with this explanation. However, it should be noted that the remaining HNO_3 (NO_3^-) and H_2O molecules, the latter of which are created in the oxidation process, still contribute to the structural expansion, resulting in the inter-nanographite-domain antiferromagnetic interaction being smaller than that of non-adsorbed ACFs. The heat-treatment at higher temperature

increases more the absolute value of the Weiss temperature, and it is larger than that of the non-adsorbed ACFs at 800 °C. In the residue compound treated around this temperature, edge carbon atoms are less decorated by bulky functional groups, and importantly the edge states are subjected to charge transfer and electronic structure modification, in which a small concentration of nitrogen strongly bonded to the edge carbon atoms and incorporated into the participating graphene sheets,[47] as evidenced by the presence of a trace of nitrogen (Fig.5(b)) and the absolute value of the orbital susceptibility being smaller than that of the non-adsorbed ACF (Fig.4b)). The edge state is localized at the zigzag edges when the Fermi energy is located at the Dirac point, while it becomes less localized at the edges and more extended to the interior of nanographene sheet when the Fermi level is shifted down from the Dirac point by charge transfer.[16] It is considered that the rather extended feature in the edge state can enhance the inter-nanographite-domain antiferromagnetic interaction, ensuing in the increase in the absolute value of the Weiss temperature in the RC-800 sample.

Finally we comment the behavior of the ESR spectra which give important information on the interaction of edge-state spins. For the non-adsorbed ACFs, residue compounds and HNO_3-ACFs, the ESR spectra show one single Lorentzian-shaped curve, indicating the edge-state spins are coupled with each other through exchange interaction. The derived linewidth (ΔH_{pp}) is plotted as a function of heating temperature in the Figure 4(f). When the heating temperature increases from 200 °C to 800 °C, the ΔH_{pp} of the non-adsorbed ACFs increases from ~5 mT to ~22 mT. This could be explained in terms of strengthening the exchange interaction within the individual nanographene sheet. According to the previous report, fast electron hopping at room temperature between nanographene sheets makes the inhomogeneous line width of inter-nanographene-sheet interaction origin disappear due to motional narrowing.[33] As a result, the line width can be explained only in terms of intra-nanographene-sheet interaction (intra-zigzag-edge and inter-zigzag-edge interactions). The line width here obeys the Korringa relation;[48] the line width is inversely proportional to the square of the interaction $J_{\pi\text{-edge}}$ between the edge-state spin and the conduction π-electron spin. The strength of $J_{\pi\text{-edge}}$ increases as the Fermi level approaches the Dirac point upon the decrease in charge transfer with the oxygen-containing functional groups. Consequently the line width increases as the heating temperature is elevated, as we see in the experimental result shown in Fig. 4(f).

In the residue compounds, the increase in the line width is weaker than that in the non-adsorbed ACFs. This can be related to the charge transfer to a trace of oxygen/nitrogen-containing functional groups strongly bonded to the edge carbon atoms even at 800 °C. The Fermi level slightly downshifted from the Dirac point weakens the strength of $J_{\pi\text{-edge}}$, resulting in the line width narrower than that in the non-adsorbed ACF at the same temperature.

4. Conclusion

As an important feature in nanographene, the graphene edge is chemically, electronically and magnetically active due to the presence of nonbonding edge state having a large local density of states with a localized spin. As the edge state is located at the Dirac point, at which the conduction π and valence π* band touch each other, the magnetic and electronic properties of nanographene are seriously affected by charge transfer. By using nanographene-based nanoporous host ACFs, the electronic properties together with the behavior of edge state are examined through element analysis, SQUID, NEXAFS and ESR spectra in relation to the host-guest interaction with HNO_3 as acceptor-type guest and its vacuum-heat-treatment effect.

The adsorption of HNO_3 into ACFs depresses the edge-state contribution to the electronic properties owing to the charge transfer from nanographene to acceptor HNO_3 molecules, which are intercalated in the galleries of nanographene sheets and also adsorbed in the nanopores between the nanographite domains. In addition, a part of the adsorbed HNO_3 molecules are decomposed with the aid of electron-rich edge state as oxidation catalyst into oxygen/nitrogen-containing functional groups bonded to edge carbon atoms of nanographene and magnetic NO molecules as a result of the oxidation of graphene edges. This change upon HNO_3 adsorption is tracked in the behavior of magnetic properties; the decrease in the orbital susceptibility, the decrease in the edge-state spin concentration and the creation of additional magnetic NO molecules.

The evacuation of the HNO_3-ACFs at 200 °C can remove the HNO_3 molecule species due to its bad thermal stability, producing a residue compound, in which a part of oxygen/nitrogen-containing functional groups remain still bonded. The further heating up to 800 °C under vacuum cannot remove a trace of nitrogen-containing species strongly bonded to the nanographene edges, and accordingly it cannot free the edge-state spins from the charge transfer and electronic structure modification induced by the residual oxygen/nitrogen-containing species. The presence of such oxygen/nitrogen-containing species, which is evidenced by the orbital susceptibility weaker than that of the pristine ACFs, makes the edge state less localized, resulting in the enhancement of the inter-nanographite-domain antiferromagnetic interaction and the weakening of the intra-nanographene-sheet exchange interactions..

Acknowledgement

The authors are grateful for the financial support of the Grant-in-Aid for Scientific Research No. 20001006 from MEXT. The present work has been performed under the approval of Photon Factory Program Advisory Committee (PF-PAC 2010G036).

Notes

[a]*Department of Chemistry, Tokyo Institute of Technology, 2-12-1 Ookayama Meguro, Tokyo 152-8551, Japan*
mail: kiguti@chem.titech.ac.jp, tenoki@chem.titech.ac.jp
[b]*DENSO CORPORATION, Research Laboratories: 500-1, Minamiyama Komenoki-cho, Nisshin-shi, Aichi 470-0111, Japan*
[†] *Present address: Department of Chemical Science and Technology, Faculty of Bioscience and Applied Chemistry, Hosei University, 3−7−2 Kajino-chou, Koganei, Tokyo 184−8584, Japan.*

References

1 K. S. Novoselov, A. K. Geim, S. V. Morozov, D. Jiang, Y. Zhang, S. V. Dubonos, I. V. Grigorieva, and A. A. Firsov, *Science* 2004, **306**, 666-669.
2 K. S. Novoselov, D. Jiang, F. Schedin, T. J. Booth, V. V. Khotkevich, S. V. Morozov, and A. K. Geim, *Proc. Natl. Acad. Sci. U.S.A*. 2005, **102**, 10451-10453.
3 A. H. Castro Neto, F. Guinea, N. M. R. Peres, K. S. Novoselov, and A. K. Geim, *Rev. Mod. Phys*. 2009, **81**, 109-162.
4 D. S. L. Abergel, V. Apalkov, J. Berashevich, K. Ziegler, and T. Chakraborty, *Adv. Phys*. 2010, **59**(4), 261-482.
5 N. Levy, S. A. Burke, K. L. Meaker, M. Panlasigui, A. Zettl, F. Guinea, A. H. Castro Neto, and M. F. Crommie, *Science* 2010, **329**, 544-547.
6 Y. Shao, J. Wang, H. Wu, J. Liu, I. A. Aksay, and Y. Lin, *Electroanalysis* 2010, **22**, 1027-1036.
7 F. Xia, D. B. Farmer, Y.-M. Lin, and P. Avouris, *Nano Lett*. 2010, **10**, 715-718.
8 L. Qu, Y. Liu, J.-B. Baek, and L. Dai, *ACS Nano* 2010, **4**, 1321-1326.
9 W. Yang, C. He, L. Zhang, Y. Wang, Z. Shi, M. Cheng, G. Xie, D. Wang, R. Yang, D. Shi, and G. Zhang, *Small* 2012, **8(9)**, 1429-1435.
10 L. Chen, Y. Hernandez1, X. Feng, and K. Müllen, *Angew. Chem. Int. Ed.* 2012, 51(31), 7640–7654.
11 K. Kawasumi, Q. Zhang, Y. Segawa, Lawrence T. Scott, and K. Itami, *Nature Chem*. 2013, **5**, 739–744.
12 K. Yang, L. Feng, X. Shi, and Z. Liu, *Chem. Soc. Rev.* 2013, **42(2)**, 530-547.
13 K. Tanaka, S. Yamashita, H. Yamabe, and T. Yamabe, Synth. *Met*. 1987, **17**, 143-148.
14 S. E. Stein and R. L. Brown, *J. Am. Chem. Soc.* 1987, **109**, 3721-3729.
15 M. Fujita, K. Wakabayashi, K. Nakata, and K. Kusakabe, *J. Phys. Soc. Jpn*. 1996, **65**, 1920-1923.
16 M. Fujita, M. Igami, and K. Nakada, *J. Phys. Soc. Jpn.* 1997, **66**, 1864-1867.
17 K. Nakada, M. Fujita, G. Dresselhaus, and M. S. Dresselhaus, *Phy. Rev. B* 1996, **54**, 17954-17961.
18 K. Wakabayashi, M. Fujita, H. Ajiki, and M. Sigrist, *Phys. Rev. B* 1999, **59**, 8271-8282.
19 T. Enoki, M. Suzuki, and M. Endo, *Graphite Intercalation Compounds and Applications*, Oxford University Press, New York, 2003.
20 Y. Kobayashi, K. Fukui, T. Enoki, K. Kusakabe, and Y. Kaburagi, *Phys. Rev. B 2005,* **71**, 193406.
21 K. Sakai, K. Takai, K. Fukui, T. Nakanishi, and T. Enoki, *Phys. Rev. B* 2010, **81**, 235417.
22 Y. Niimi, T. Matsui, H. Kambara, K. Tagami, M. Tsukada, and H. Fukuyama, *Phys. Rev. B* 2006, **73**, 085421.
23 K. Suenaga and M. Koshino, *Nature* 2010, **468**, 1088.
24 P. Esquinazi, A. Setzer, R. Höhne, C. Semmelhack, Y. Kopelevich, D. Spemann, T. Butz, B. Kohlstrunk, and M. Lösche, *Phys. Rev. B* 2002, **66**, 024429.
25 P. Esquinazi, D. Spemann, R. Höhne, A. Setzer, K. -H. Han, and T. Butz, *Phys. Rev. Lett*. 2003, **91**, 227201.
26 S. Entani, S. Ikeda, M. Kiguchi, K. Saiki, G. Yoshikawa, I. Nakai, H. Kondoh, and T. Ohta, *Appl. Phys. Lett*. 2006, **88**, 153126.
27 E. Velez-Fort, M. G. Silly, R. Belkhou, A. Shukla, F. Sirotti and A. Ouerghi, *Appl. Phys. Lett.* 2013, **103**, 083101.
28 V. L. J. Joly, M. Kiguchi, S.-J. Hao, K. Takai, T. Enoki, R. Sumii, K. Amemiya, H. Muramatsu, T. Hayashi, Y. A. Kim, M. Endo, J. Campos-Delgado, F. López-Urías, A. Botello-Méndez, H. Terrones, M. Terrones, and M. S. Dresselhaus, *Phys. Rev. B* 2010, **81**, 245428.
29 M. Kiguchi, K. Takai, V. L. J. Joly, T. Enoki, R. Sumii, and K. Amemiya, *Phys. Rev. B* 2011, **84**, 045421.
30 K. Kaneko, C. Ishii, M. Ruike and H. Kuwabara, *Carbon* 1992, **30**, 1075-1088.
31 Y. Shibayama, H. Sato, T. Enoki, X. X. Bi, M.S. Dresselhaus, and M. Endo, *J. Phys. Soc. Jpn.* 2000, **69**, 754-767.
32 T. Enoki and K. Takai, *Solid. State. Commun*. 2009, **149**, 1144-1150.
33 V. L. J. Joly, K. Takahara, K. Takai, K. Sugihara, M. Koshino, H. Tanaka, T. Enoki, *Phys. Rev. B* 2010, **81**, 115408.
34 H. Sato, N. Kawatsu, T. Enoki, M. Endo, R. Kobori, S. Maruyama, and K. Kaneko, *Solid. State. Commun.* 2003, **125**, 641-645.
35 H. Sato, N. Kawatsu, T. Enoki, M. Endo, R. Kobori, S. Maruyama, and K. Kaneko, *Carbon* 2007, **45**, 214-217.
36 K. Takai, H. Kumagai, H. Sato, and T. Enoki, *Phys. Rev. B* 2006, **73**, 035435.
37 K. Takai, S. Eto, M. Inaguma, T. Enoki, H. Ogata, M. Tokita, and J. Watanabe, *Phys. Rev. Lett*. 2007, **98**, 017203.
38 S. -J. Hao, K. Takai, F. -Y. Kang, and T. Enoki, *Carbon* 2008, **46**, 110-116.
39 S.-J. Hao, K. Takai, V. L. Joseph Joly, K. Yokota, M. Kiguchi, and T. Enoki, *Bull. Chem. Soc. Jpn*. 2012, **85**(3), 376-388.
40 E. W. Washburn, *International critical tables of numerical data, physics, chemistry and technology*, McGraw-Hill, New York, 1928, vol. 3, pp. 301-305.
41 J. Stohr, NEXAFS Spectroscopy, Springer, New York, 1991.
42 Kuraray Technical Report, http://www.kuraraychemical.com/Technical/Kuraactive/Kuraactive.htm, (Accessed January 2014).
43 P. Leinweber, J. Kruse, F. L. Walley, A. Gillespie, K.-U. Eckhardt, R. Blyth, and T. Regier, *J. Synchrotron Rad.* 2007, **14**, 500-511.
44 G. U. Sumanasekera, G. Chen, K. Takai, V. L. J. Joly, N. Kobayashi, T. Enoki, and P. C. Eklund, *J. Phys.: Condens. Matter*. 2010, 22, 334208.
45 D. Pacile, J. C. Meyer, A. Rodriguez, Papagno, M. Fraile, C. Gomez-Navarro, R. S. Sundaram, M. Burghard, K. Kern, C. Carbone, and U. Kaiser, *Carbon* 2011, **49**, 966-972.
46 M. Koshino and T. Ando, *Phys. Rev. B* 2010, **81**, 195431.
47 S.-F. Huang, K. Terakura, T. Ozaki, T. Ikeda, M. Boero, M. Oshima, J.-I. Ozaki, and S. Miyata, *Phys. Rev. B* 2009, **80**, 235410.
48 J. Korringa, *Physica* 1950, **16**, 601-610.

TOC

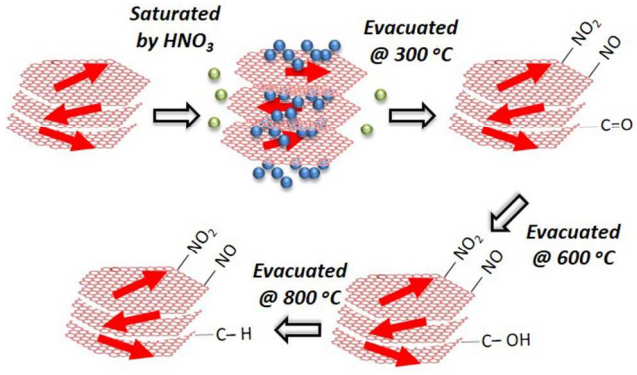

The magnetism of HNO_3 doped nanographene sheets is affected seriously through charge transfer and structural compression, but heating under vacuum leads to the recovery.